Available online at www.sciencedirect.com
ScienceDirect
Procedia Engineering 2 (2010) 2317–2326
Procedia Engineering
www.elsevier.com/locate/procedia

Fatigue 2010

Fatigue crack propagation in thin wires of ultra high strength steels

J. Petit*, C. Sarrazin-Baudoux and F. Lorenzi

ENSMA, LMPM,, P'Institute, 1 Avenue C. Ader, Chasseneuil-Futuroscope, France

Received 28 February 2010; revised 12 March 2010; accepted 15 March 2010

Abstract

Fatigue crack propagation is studied in thin wires of about 1 mm in diameter of an ultra high strength steel ($\sigma_{max} > 2400MPa$). Tests are performed on an electro linear testing machine at a frequency of 20Hz in ambient air. Crack growth is optically monitored by mean of a long distance microscope with numerical acquisition of crack images. Threshold tests are run in accordance with the load shedding technique with special new requirements to account for the specimen geometry. The influence of load ratio $R = 0.4$ *or* 0.7 and *variable* R at *constant* K_{max} is examined. The results support a substantial effect of atmosphere especially on near-threshold propagation and on the threshold of the stress intensity factor range. A substantial contribution of crack closure is put in light. The propagation data are compared to previous data on conventional high strength steels tested in air and in high vacuum with closure correction. Crack path and crack surface morphology microscopic observations allow the identification of the fatigue crack propagation mechanisms.

Keywords: cold drawn pearlitic steel; thin wire; fatigue crack propagation; threshold; load ratio; effective threshold.

1. Introduction

Drawn pearlitic steel wires are known to be extremely strong. Ultimate tensile strength σ_{max} as high as 3000 MPa can be reached this is almost ten times the tensile strength of annealed mild steel. Two main reasons can be put forward for this high strength (Verpoest et al. [1]). Pearlitic steel wires are particularly suited for industrial applications as all types of springs, reinforcements of tyres and hoses, ropes or cables.... In most of these applications, cyclic loads or deformations are predominant, and consequently it is of primary importance to study the cyclic performance of these ultra high strength steels or, in other words, their fatigue properties. Most of the papers of the available literature on that topic are devoted to high cycle fatigue behaviour of cold drawn pearlitic steel [2-9] and to corrosion fatigue [10-15], with some of them focused on the role of the microstructure with respect to the degree of cold drawing on the fatigue life. But few papers are dedicated to fatigue crack propagation and fatigue threshold [16-20], most studies being conducted on wires having a diameter of about 5 to 10 mm [17-20]. Only a very little number of studies have been carried on thin wires with diameter of about 1.5 to 2 mm [1, 15].A major obstacle is the difficulties to perform valuable experiments for the characterisation of the near-threshold fatigue crack propagation and thus for the evaluation of the fatigue threshold ΔK_{th}. On the one hand, pearlite has an intrinsically strong microstructure since it can be viewed as a lamellar composite of randomly oriented, strong but brittle cementite plates, and weak but ductile

* Corresponding author. *E-mail address*: jean.petit@ensma.fr

1877-7058
doi:10.1016/j.proeng.2010.03.248

Nomenclature

a	crack depth	K_I	stress intensity factor for mode I
D_0*	intrinsic cumulative plastic displacement	K_{max}	maximum of stress intensity factor
D*	cumulative plastic displacement	R	load ratio resistance
da/dN	crack growth rate	R_{cp}	cyclic plastic zone size
ΔK	stress intensity factor range	σ_{max}	ultimate
ΔK_{th}	threshold stress intensity factor range	σ_y	yield strength
$\Delta K_{eff,th}$	effective threshold stress intensity factor range	w	specimen width

ferrite interlayers [1,8,21-23]. The cementite lamellae are assumed acting as efficient barriers for the moving dislocations in the ferrite. On the other hand, cold deformation during wire drawing has been shown to harden the ferrite and reduce the interlamellar spacing. Moreover, the cementite lamellae gradually change their orientation, so that at a true strain $\varepsilon = 1.5$ or higher, they are almost all parallel to the wire axis; cold drawn pearlite has then become like an oriented lamellar composite, with an optimized strengthening efficiency of the cementite plates associated to a < 110> fibre texture. Moreover, as reported by Verpoest et al.[1], drawn steel wires always have a very rough surface (pits, scratches, grooves, overlaps ...). These authors underlined that initial works by De Bondt [24] identified local decarburisation spots, pickling pits, broken martensite layers and inclusions as main fatigue crack starters in drawn pearlitic steel wire. Later it the importance of inclusions in this steels was emphasized [25]. Hence, Verpoest et al., [1] postulated that, in accordance with basic works done by K. Miller et al.[26] on surface microcrack propagation, fatigue cracks in drawn pearlitic steel wires always grow from pre-existing surface defects; consequently, they suggested that the limit between growth and non-growth of cracks, which corresponds to the fatigue limit, is determined by the threshold stress intensity range ΔK_{th}. Therefore, if the pre-existing surface defects could be treated as cracks, the fatigue threshold would indicate whether or not, at an applied cyclic stress amplitude σ_a, these cracks will propagate. From the general formula

$$\Delta K_{th} = \alpha \Delta \sigma_a \sqrt{\pi a} \quad (1)$$

Then the condition for non propagation of a pre-existing crack a_0 is:

$$\sigma_a < \Delta K_{th} / (2\alpha\sqrt{\pi a}) \quad (2)$$

The present research program on thin steel wires (diameter of about 1 mm) was carried out in order to obtain an experimental determination of the near threshold fatigue crack propagation behaviour and an evaluation of the fatigue threshold to determine condition for the absence of any crack propagation on ultra high strength pearlitic steel.

2. Experimentals

The studied material is cold drawn, pearlitic steel wire ($\%C < 0.6$) with a diameter $\phi = 0.95$mm. The drawing strain ε is > 2.0 and the tensile strength is > 2400 MPa. The specimens are machined from 70mm long wires. Two opposite plane faces are machined by mean of an electrosparkling machine. Machining results in the centre of the specimen in a rectangular section of about 0.4 mm x 1.2 mm along a length of about 10mm, the two ends remaining cylindrical for gripping on the testing machine. A semi circular micro notch with a radius of 0.15mm is then machined in the middle of one side of the specimen giving finally a micro SEN specimen. Finally, the two planar opposite faces are carefully polished for optical observation, and the remaining thickness is of about 0.3 to 0.35 mm. Fatigue crack growth experiments are conducted on an electrodynamic testing machine (load capacity of 1000N), equipped with a load cell having a capacity of 250N. Tests are run under load control at a frequency of 20 Hz, the load amplitude ranging from 5 to 25N. The load ratio R is of 0.4 or 0.7, and constant K_{max} tests are also run with R increasing from 0.4 at the beginning of the test up to more than 0.9 in the near threshold region allowing to expect

the elimination of any crack closure contribution [27]. Hygrometry of the laboratory air was checked at each step of measurement. Once a crack grew to about 20 µm length, a load shedding technique is applied to obtain crack growth rates as low as some 10^{-11} m/cycle at final length of 500 to 600µm. The crack length is monitored during the test by mean of a long distance microscope recording digital pictures of the crack at each step of the propagation. The crack length is measured from these pictures with a resolution of about 1 µm. The stress intensity factor ΔK is evaluated in LEFM conditions using the geometrical correction factor of SEN specimens of relation (3), for ΔK ranging below 8 $MPam^{1/2}$ when the plastic zone size for such very high strength material is sufficiently small.

$$f(a/w) = 5/ [20-13(a/w)-7(a/w)^2]^{1/2} \quad (3)$$

This relation has been validated by mean of FEM calculation for $0.2 < a/w < 0.55$.

3. Results

3.1. Fatigue crack propagation and threshold

The figures 1a and 1b show results for crack propagation rate evolution with respect to the stress intensity factor range in a double logarithmic diagram for tests respectively run at $R=0.4$ and $R=0.7$ at a frequency of 20 Hz in laboratory air with a residual humidity ranging between 35% an 55%. In all cases, a typical change of slope in the curve da/dN *vs* ΔK can be observed for da/dN about 10^{-9} m/cycle.

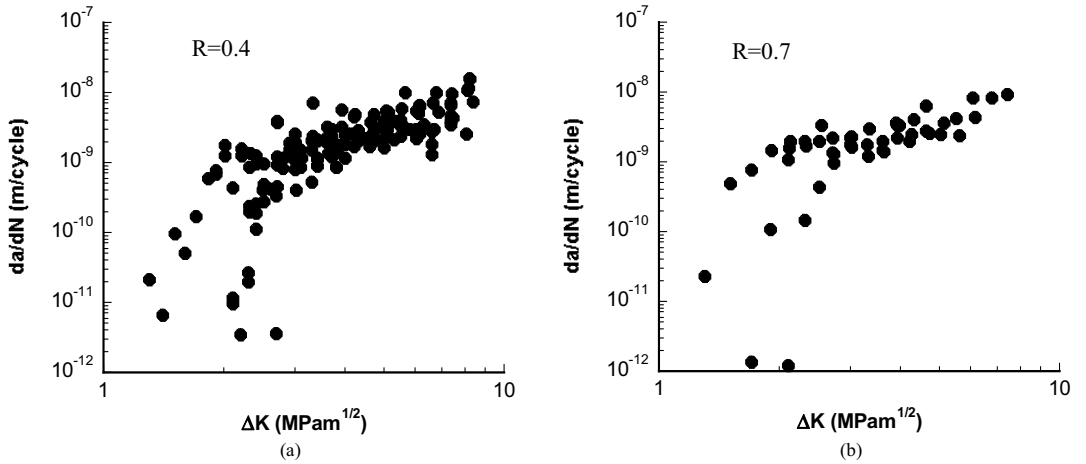

Fig. 1. da/dN *vs* ΔK bi logarithmic diagram for propagation data of tests run at 20 Hz in air (35 to 55% RH) on 0.58%C pearlitic thin steel wires (diameter 0.95mm): (a) $R=0.4$ and (b) $R=0.7$.

For greater values of da/dN, whatever the R *ratio* all the data fall in the same scatter band (figure 2) and the material follows a power law of the type of the Paris law as:

$$da/dN = C\,\Delta K^m \quad (4)$$

The absence of influence of the R ratio in the upper ΔK range of figures 1a and 1b, is consistent with the absence of closure for R= or > 0.4 in the Paris regime as generally observed on metallic alloys [27].

For lower values of da/dN, the first characteristic is a large scatter in the results and particularly for the threshold ΔK_{th} range. From one specimen to the other ΔK_{th} can be reduced (or augmented) about 2 times. However, the

growth rates globally are faster and the threshold is lower at R=0.7 compared to R=0.4. In opposition with the behavior at higher growth rates indicating a propagation without contribution of crack closure for R = or > 0.4, the near threshold domain is characterized by a substantial contribution of crack closure, this contribution being variable from one specimen to the other whatever the R ratio. These results suggest a huge contribution of residual stresses induced by the cold work process [1, 20] and also by the initial curvature of the specimens which compensated by the loading. The curvature fine steel wires is the reason why tests must be run at R *ratio* equal or higher than 0.4 when one want to avoid bending of the specimen during the cyclic loading. To validate this analysis on the contribution crack closure, a *constant* K_{max} test is performed, allowing reaching the near threshold domain with load ratio of about 0.9. The crack growth data obtained in such conditions are compared in figure 2 to data of figures 1a and 1b. Clearly, the *constant* K_{max} test gives the lower boundary for the resistance of the material against fatigue crack propagation. The corresponding threshold is the effective threshold range for the atmospheric environment:

$$\Delta K_{eff,\,th} = 1.1 \text{ MPam}^{1/2}. \quad (5)$$

When the design of an element or a component of a structure would prevent the propagation of fatigue cracks, this threshold value has to be considered.

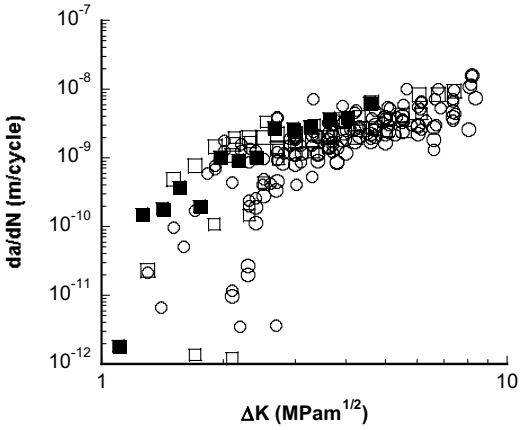

Figure 2: Comparison of *da/dN vs ΔK* diagram for tests run at *constant* K_{max} , R=0.4 and R=0.7

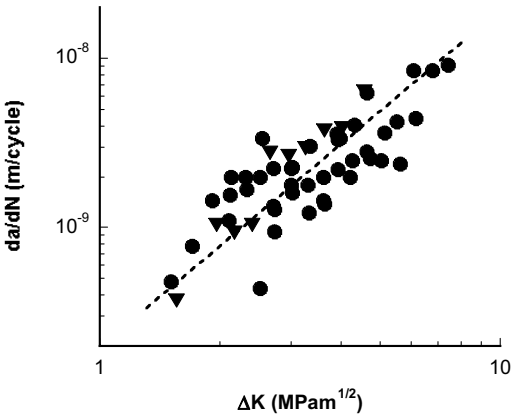

Figure 3: Crack propagation data for tests run at R=0.7 or at *constant* K_{max} at *da/dN* > 5.10^{-10} m/cycle; the dotted line corresponds to a *ΔCTOD* controlled mechanism with a slope m=2.

The data of tests run at *constant* K_{max} and R=0.7 at growth rate higher than 5.10^{-10} m/cycle are plotted in figure 3. They are consistent with a propagation law of the type of relation (4) with an exponent m = 2 in accordance with a Crack Tip Opening Range *ΔCTOD* controlled crack propagation as initially described by Pelloux [43].

3.2. Fracture surface morphology

The fracture surfaces of the fatigue cracks are illustrated in figures 4 and 5 comparing the surface morphology at the beginning of the threshold tests (figure 4) to that in the near threshold area (figure 5). The fatigue crack grows across the section of the wire in a plane normal to load axis which is typical of stage II cracks (figure 4a).

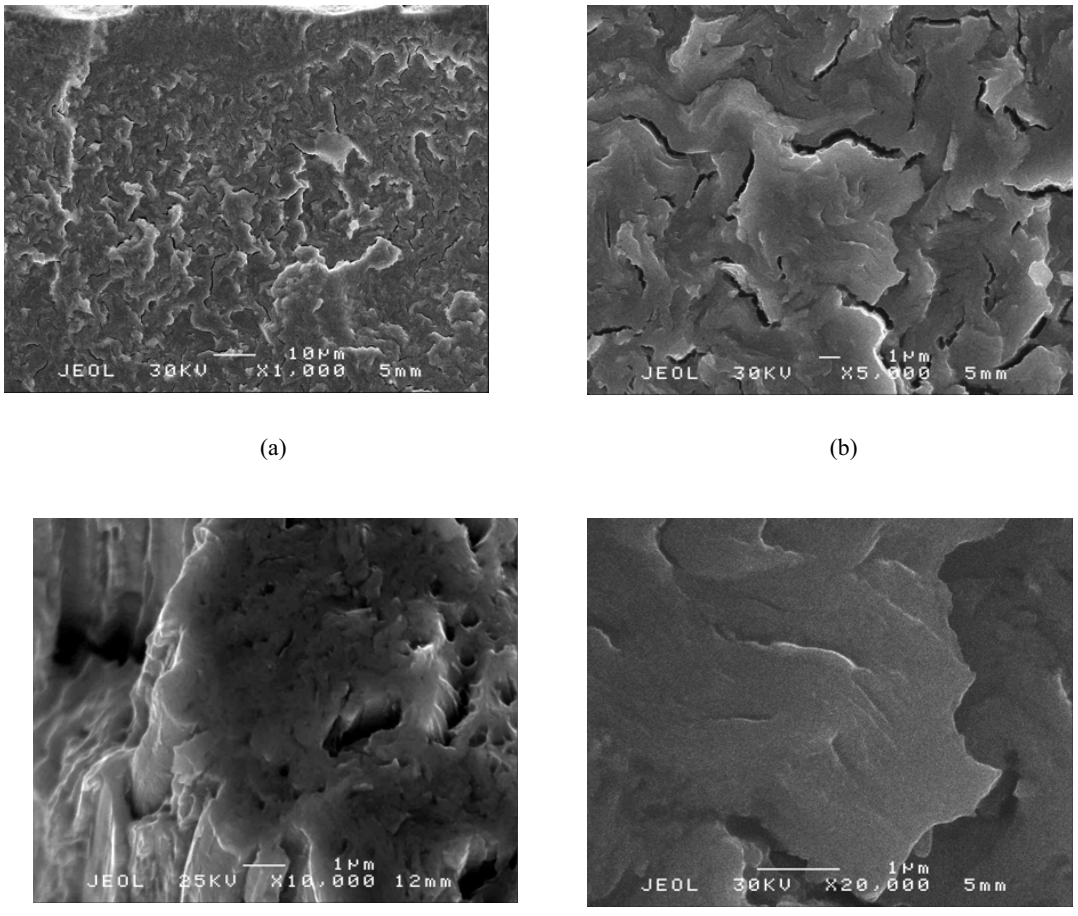

(a) (b)

(c) (d)

Figure 4: SEM observations of the fracture surface for test run at R=0.4: (a) initial propagation at the tip of the notch machined by mean of electrosparkling; (b) microfractography at ΔK= 6MPam$^{1/2}$, da/dN= 3.10^{-9} m/cycle; (c) final rupture at the end of the fatigue crack path showing the fibrous axial microstructure; (d) magnification of (b).

The crack initiation seems to correspond to a narrow facetted area (top of figure 4a) corresponding to a localized initial stage I expending along a depth of about the size of 2 to 3 grains size in the cross section. In the figure 4b, a micrograph of the beginning of the final rupture just at the end of the fatigue crack path shows the relation between

the grained aspect of the cross section as shown in figure 4b and the longitudinal fibrous texture of the microstructure. This figure supports also that the microcracks observed around the grains can result from a longitudinal delaminating damage process even during the fatigue crack progression before the final rupture. In figure 4d, a magnification of the crack path in the grained structure is consistent with a crack growth mechanism resulting from a cumulative plastic deformation and a step by step crack advance, the growth rate being too slow for a cycle by cycle crack progression with associated striations. In the near threshold domain ($da/dN<10^{-10}$ m/cycle) the fracture surface is flat essentially marked by microcracks at the grain boundaries, the stage II transgranular propagation being essentially featherless. Such smooth surface can be a consequence of low deformation associated to low stress intensity factor range. But in addition, on the basis of the analysis presented here above supporting a substantial contribution of crack closure in the near-threshold domain even at R=0.7, such surface aspect can also result a from drastic reduction of the surface roughness induced by a fretting and erosion process between the two lips of the crack when it is fully closed at each cycle [17]. The particles pulled out by the friction may fill up the microcracks and thus accentuate the smoothness of the surface. It is valuable to notice that in such ultra high strength steel the crack tip opening displacement $CTOD$ for ΔK=2MPam$^{1/2}$ can be estimated from the following expression [28]:

$$CTOD = K_I^2/\sigma_y E \qquad (6)$$

Table 1. $CTOD_{max}$ and $\Delta CTOD$ versus R ratio for ΔK =2 MPam$^{1/2}$

R	K_{max}	$CTOD_{max}$	$\Delta CTOD$
0.0	2.00	8.34 nm	4.17 nm
0.4	3.33	23.2 nm	4.17 nm
0.7	6.67	92.7 nm	4.17 nm
0.9	20.00	834 nm	4.17 nm

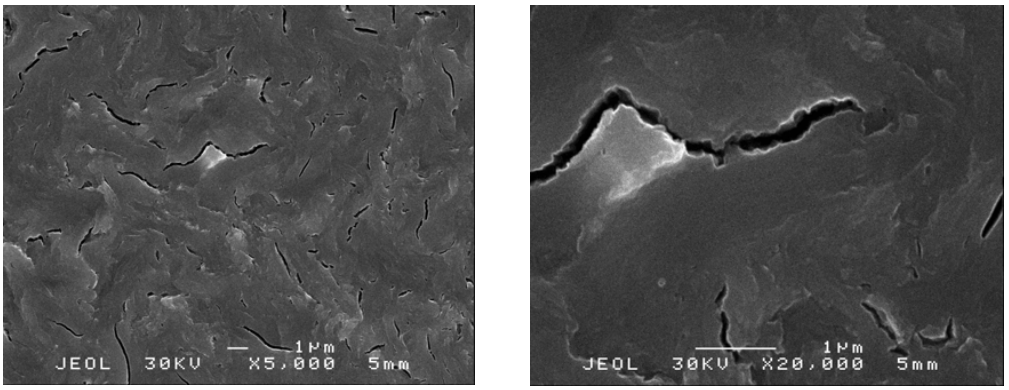

(a) (b)

Figure 5: SEM observations of the fracture surface for test run at R=0.4: (a) microfractographic aspect of the near threshold area: da/dN = 3.10^{-11} m/cycle; (b) magnification of (a).

The values of the $CTOD$ for the maximum load, $CTOD_{max}$, and of the $CTOD$ range $\Delta CTOD$ during a loading cycle are given in Table 1 interlamellar spacing of about 15 nm). It is understandable that roughness induced closure is

difficult to ovoid, except for high *R ratio* (= or > 0.9) for which $CTOD_{max}$ becomes about 1 µm. For example, for the threshold test conducted at *constant* K_{max}, the lowest ΔK *is* 1.1 MPam$^{1/2}$ which means a very small $\Delta CTOD$ of 1.2 nm, but at the same time, with R=0.916, the $CTOD_{max}$=1.18µm and hence the crack is expected to be open during all the loading cycle. These $\Delta CTOD$ and $CTOD_{max}$ values can be compared to the interlamellar spacing of the eutectoid pearlitic microstructure which is about 70 nm. It is noticeable that the change in the slope of the propagation curve, when one reaches the near threshold domain, corresponds to ΔK ranging about 3 to 2 MPam$^{1/2}$ (figure 1), and $\Delta CTOD$ ranging about 8 to 18 nm, which means smaller than the interlamellar spacing. The change in the slope is also expected to correspond to the appearance of a contribution of crack closure. Hence, it could be postulated that crack closure, suspected to be induced by the surface micro-roughness, can become operative when the ΔCTOD is smaller than the interlamellar spacing. On another hand, the cyclic plastic zone size can be estimated from the following relation [28]:

$$R_{cp} = 8/\pi(K_I/\sigma_y)^2 \quad (6)$$

At the change in the slope of the propagation curves, R_{cp} *= 50 to 120 nm*. In the near threshold domain R_{cp} is of the same size as the interlamellar spacing, and the plastic deformation is well localized within individual grain all along the crack front. Considering the very small size of the microstructure components and of the plastic zone, these results do not help in making a decision for the origin of crack closure which could be induced as well by localized plasticity or by micro-roughness, or a combination of both mechanisms.

3.3. Threshold

In figure 6 are plotted the results obtain for ΔK_{th}, the threshold stress intensity factor range, with respect to R in this study and compared to data provided by the literature for pearlitic steels having an ultimate strength higher than 1600 MPa [1, 15, 29, 30]. In conventional pearlitic steels, the two main characteristics of the microstructure which can affect crack closure are the austenitic grain size and the interlamellar spacing of the pearlite [16, 18]. Large

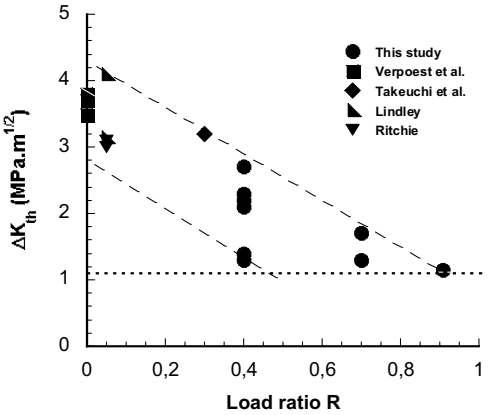

Figure 6: ΔK_{th} dependence with R (Verpoest et al. [1], Takeuchi et al.[15], Lindley [29], Ritchie [30]).

austenitic grain sizes as well as high pearlite interlamellar distance produce rougher crack surfaces, increasing the crack closure effect, leading to quite high threshold ranging between 8 and 10 MPam$^{1/2}$ at low R ratio. The scatted is wide particularly for the lower R ratio. However the general trend is a decrease of ΔK_{th} with increasing R as generally shown for metallic materials [ref] and previously noticed for high strength cold drawn eutectoid steel wires [1, 16, 18]. For R ratio higher than 0.4 the threshold can be reached without closure, probably because of residual stresses. A conservative evaluation of the fatigue limit for R < 0.4 can done from the lower boundary envelop, and for R > 0.4 the effective threshold $\Delta K_{eff,th}$ can be recommended. The value of this effective threshold is very low as compared to threshold values commonly obtained on pearlitic steels (higher than 5 MPam$^{1/2}$). But

similar low $\Delta K_{eff,th}$ have been reported on various metallic materials including Al and Ti based alloys for tests conducted in ambient air or in humidified atmosphere in contrast with $\Delta K_{eff,th}$ in high vacuum which is considered as a reference for an inert environment [34]. A complete understanding of the near-threshold fatigue crack growth behaviour of the studied steel requires an insight in the influence of the ambient environment.To document the atmosphere influence, thorough analyses of the fatigue crack growth rate as a function of environment have been performed with systematic crack closure correction on various metallic alloys [35], in ambient air, in inert gas with controlled partial pressure of water vapor, and in high vacuum. Some main characteristics of atmosphere environment effect on fatigue crack propagation have been brought out:

i) a detrimental effect of atmosphere water vapor on most of metals and metallic alloys;
ii) a pronounced atmosphere effect at low growth rate in the low stress intensity factor range;
iii) a characteristic influence on fracture surface morphology;
iv) a complexe interrelation between environment and microstructure.

For fatigue crack propagation in steels, the stage II mode with the activation of different slip systems leading to homogeneous deformation and smooth crack path, has been shown predominant as well in active environment as under vacuum, and three distinct stage II regimes have been identified:

i) in high vacuum the intrinsic stage II prevails, and can be described with a propagation law derived by Petit et al. [34] from the initial model of Rice [37]or Wertmann [38] as:

$$da/dN = A/D_0^*[\Delta K_{eff}/E]^4 \tag{7}$$

where A is a dimensionless parameter and D_0^* the critical cumulated displacement.
Examples of intrinsic propagation are given in figure 7 for comparison purpose and to evaluate the influence of environment when the crack grows in air.

ii) in moist atmospheres including ambient air, a stage II propagation regime assisted by water vapor adsorption [34, 38-40] which can be described with a relation derived from relation (7) as follows [34,39] where D^* is the cumulative displacement in an active environment:

$$(da/dN)_{ad} = A/D^*[\Delta Keff/E]^4 \tag{8}$$

The physical adsorption of water vapor molecule on fresh surfaces at the crack tip diminishes the energy required for the creation of a new crack surface [26], and thus is assumed to reduce the cumulative plastic deformation D^* within the process zone and thus accelerate the growth rate without changing the basic mechanism.

iii) a hydrogen assisted stage II propagation [34, 38, 41, 42], hydrogen being provided from the chemical dissociation of adsorbed water vapor molecules. This regime can be described with a relation derived by Petit et al. [34] from the initial model for $\Delta CTOD$ controlled propagation [43] written as:

$$da/dN = B[\Delta K_{eff}^2/E\sigma] \tag{9}$$

where B is a dimensionless coefficient and σ a strength parameter.

Critical conditions for the occurrence of hydrogen-assisted propagation, depend on hydrogen concentration into the process zone, and thus depend on a ΔK range sufficiently low for achieving a quasi stationary crack with a localized plastic deformation and the attainment of critical values for parameters controlling the number of molecules of water vapor required to create an instantaneous adsorbed mono-layer (partial pressure in the surrounding of the specimen, frequency, growth rate, R ratio..). In such conditions, the kinetics of environment fatigue crack propagation is controlled by crack tip surface chemical reaction to produce oxide-based compounds plus atomic hydrogen and diffusion of hydrogen in the process zone which means a reaction-controlled mechanism as described by Wei et al. [41]. On the basis of this modeling framework for atmosphere assisted fatigue crack propagation, a compilation of data for stage II propagation in various metallic alloys can be done as illustrated in figure 7. This diagram shows that the fatigue crack propagation behavior of all metallic material can be rationalized in term of $\Delta K_{eff}/E$ [35, 44].

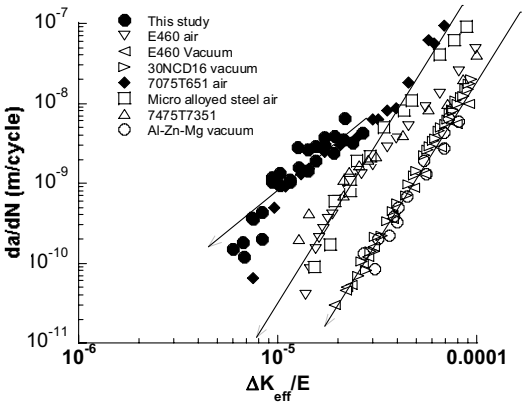

Figure 7: *da/dN* vs $\Delta K_{eff}/E$ diagram comparing data for various alloys in comparison with modeling of atmosphere assisted stage II propagation [44, 45].

The studied ultra-high strength pearlitic steel presents a crack propagation behavior in accordance with a full assistance of the atmosphere, and following this model framework, this assistance can be attributed to hydrogen provided by atmosphere water vapor, especially when the test is performed at constant K_{max} in condition without closure. It would be of interest to check out if this sensitivity to atmosphere is related to the pearlitic microstructure in itself or to some specificity of the fibrous microstructure of cold drawn wires.

4. Conclusions

Fatigue crack growth experiments have been successfully conducted on very thin wires (ϕ = 0.95mm) of an ultra high strength cold drawn pearlitic steel. The following conclusions can be brought out:

- LEFM can be used to describe the propagation rate for ΔK ranging below 8MPam$^{1/2}$;
- Crack closure contribution is shown substantial even at R ratio > 0.7;
- Near the threshold, the $\Delta CTOD$ range is much smaller than the interlamellar spacing of pearlite; thus, it is difficult to distinguish roughness- from plasticity-induced closure contribution at such very small scale;
- The effective threshold stress intensity factor range $\Delta K_{eff,th}$ determined from at very high R>0.9 *in condition assumed to be without closure is* about 1.1 MPam$^{1/2}$.
- The near threshold fatigue crack propagation can be rationalized in term of $\Delta K_{eff}/E$, and is in accordance with a $\Delta CTOD$ controlled propagation assisted by hydrogen provided by the atmospheric water vapor.

References:

[1] Verpoest I, Aernoudt E, Deruyttere A, De Bondt M. The fatigue threshold, surface condition and fatigue limit of steel wire. *International Journal of Fatigue*, 1985;**7**:199-214.
[2] Llorca J, Sanchez-Galvez V. Fatigue limit and fatigue life prediction in high strength cold drawn eutectoid steel wires. *Fatigue & Fracture of Engineering Materials & Structures*, 1985;**12**:31 – 45
[3] Beretta S, Boniardi M and Matteazzi S. Fatigue behaviour of rope eutectoid steel wires. *Zeitschrift für Metallkunde*, 1994;**85**:282-287.
[4] Kuroshima Y, Harada S, Ogawa K, Isaji M. Fatigue properties of very thin steel wire under fluctuating tension. *International Journal of Fatigue*, 1996;**18**:606-606
[5]Beretta S, Boniardi M. Fatigue strength and surface quality of eutectoid steel wires. *International Journal of Fatigue*, 1999; **21**:329-335.
[6] Chapetti MD, Miyata H, Tagawa T, Miyata T, Fujioka M. Fatigue strength of ultra-fine grained steels. *Materials Science and Engineering A*, 2004; **381**:331-336.
[7] Sun W.X., Nishida S, Hattori N, Usui I. Fatigue properties of cold-rolled notched eutectoid steel. *International Journal of Fatigue*, 2004;26:1139-1145

[8] Toribio J, González B, Matos JC, Ayaso FJ, Multi-Scale Approach to the Fatigue Crack Propagation in High-Strength Pearlitic Steel Wires, *Journal of ASTM International*, 2008;5.
[9] Yang Y.S, Bae J.G, Park C.G. Improvement of the bending fatigue resistance of the hyper-eutectoid steel wires used for tire cords by a post-processing annealing. *Materials Science and Engineering: A*, 2008;**488**:554-561
[10] Waterhouse R.B, Taylor D.E, The relative effects of fretting and corrosion on fatigue strength of an eutectoid steel.*Wear*, 1970;**15**,449-451.
[11] Raj Narayan, Ashok Kumar, K.P. Singh, The anodic polarization and stress corrosion cracking of eutectoid steel. *Corrosion Science*, 1985;**25**:449-460
[12] Takeuchi M, Waterhouse R.B, Mutoh Y and Satoh T. The behaviour of fatigue crack growth in the fretting-corrosion-fatigue of high tensile roping steel in air and seawater. *Fatigue Fract. Engng Mater. Struct*., 1991;**14**:69-77
[13] Topic M, Allen C, Tait R. The effect of cold work and heat treatment on the fatigue behaviour of 3CR12 corrosion resistant steel wire. *International Journal of Fatigue*, 2007;**29**:49-56
[14] Proverbio E, Longo P. Sub critical crack growth in hydrogen assisted cracking of cold drawn eutectoid steel. *Corrosion Science*, 2007;49:2421-2435.
[15] Shun-ichi Nakamura, Keita Suzumura, Hydrogen embrittlement and corrosion fatigue of corroded bridge wires. *Journal of Constructional Steel Research*, 2009;**65**:269-277.
[16] Llorca J, Sanchez-Galvez V. Fatigue Threshold Determination in High Strength Cold Drawn Eutectoid Steel Wires. *Eng. Fract. Mech*. 1987; **26**:869-882.
[17] Beretta S and Matteazzi S. Short crack propagation in eutectoid steel wires. *International Journal of Fatigue*, 1996; **18**:451-456.
[18] Sato T, Katagiri K, Konno K, Shoji Y, Takahashi H, Sasaki S a,d Tashiro H. Fatigue crack propagation characteristics in drawn eutectoid steels, 65 巻 638 号(1999-10) 日本機械学会論文集(A 編) ; 1999:2092-2098.
[19] El-Shabasy A.B, Lewandowski J.J. Effect of load ratio, R, and test temperature on fatigue crack growth of fully pearlitic eutectoid steel (fatigue crack growth of pearlitic steel). *International Journal of fatigue*, 2006;26:305-309.
[20] Toribio J, González B, Matos JC. Micro and macro analysis of the fatigue crack growth in pearlitic steels. *Ciência e Tecnologia dos Materiais*, 2008;**20**:68-74.
[21] Min Bae C, Long Nam W, Soo Lee C. Effect of interlamellar spacing on the delamination of pearlitic steel wires. *Scripta Materialia*, 1996;**35**:641-646.
[22] Toribio J, Delamination fracture of prestressing steel: an engineering approach. *Engng Fract. Mech.,* 2008;**75**:2683-2694.
[23] Yang Y.S, Bae J.G, Park C.G. Nanostructure and mechanical properties of heavily cold-drawn steel wires, *Materials Science and Engineering: A*, 2009;**508**:148-155.
[24] De Bondt M. Wire defects in steel reinforced rubber products. *Wire Journal*,1974:107-114.
[25] Demeyere E.G. Influence of non metallic inclusions in high- and low carbon wire rod on warkability during wire-drawing and on mechanical properties of product. Wire Journal;1981:72-77.
[26] Miller K. J, De Los Rios E. R. The Behaviour of Short Fatigue Cracks. *Mechanical Engineering Publications* Limited, London, U.K. 1986.
[27] Newman Jr.] J.C and Elber W. *ASTM STP 982: Mechanics of Fatigue Crack Closure.* American Society for Testing and Materials Pub., Philadelphia, USA, 1988.
[28] Suresh S. Fatigue of materials. Cambridge *Solid State Science Series*, Cambridge university Press, USA; 1991.
[29] Lindley T.C, Richards C.E. Near threshold fatigue crack growth in materials used in the electricity supply industry. *Fatigue Threshold*, EMAS pub., UK, 1981.
[30] Ritchie R.O. Influence of microstructure on near-threshold fatigue crack propagation in ultra-high strength steel. *Metals Science*, 1977;11:368.
[31] Backlund J, Blom A. F and Beevers C. J. *Fatigue Threshold.* EMAS Pub. 1982.
[32] Davidson D. L and Suresh S. Fatigue Crack Growth Threshold Concepts. *The Metallurgical Society of AIME Pub*., Philadelphia, Pa, USA,1984.
[33] Newman Jr, J.C and Piascik R. S. *ASTM STP 1372:Fatigue Crack Growth Threshold, Endurance Limits and Design*. American Society for Testing and Materials Pub., Philadelphia, Pa, USA. 2000.
[34] Petit J. Hénaff G. and Sarrazin-Baudoux C. Mechanisms and Modeling of Near-Threshold Fatigue Crack Propagation. *ASTM STP 1372: Fatigue Crack Growth Threshold, Endurance Limits and Design*, Newman Jr. J. C and Piascik R. S, Eds. American Society for Testing and Materials, Philadelphia, Pa, USA; 2000:3-30.
[35] Petit J. and Hénaff G. Stage II intrinsic fatigue crack propagation. *Scripta Metall.,* 1991;**25**:2683-2687.
[36] Rice, J. R. Plastic Yielding at a crack Tip. *Proceeding of International Conference on Fracture,* Sendaï Japan, 1965:283-308.
[37] Weertman J. Rate of Growth of Fatigue Cracks Calculated from the Theory of Infinitesimal Dislocations Distributed on a Plane. *International Journal of Fracture Mechanics*, 1966;**2**:460-467.
[38] Henaff G, Marchal K and Petit J. On fatigue crack propagation enhancement by a gaseous atmosphere: Experimental and theoretical aspects. *Acta Metall Mater.,*1995;**43:**2931-2942.
[39] S. P.Lynch. Environmentally assisted cracking: overview of evidence for an adsorption-induced localized-slip process. *Acta Met.*1988;36: 2639.
[40] Bouchet B, de Fouquet J and Aguillon M. Influence de l'environnement sur les facies de rupture par fatigue d'éprouvettes monocristallines et polycristallines d'alliage Al-Cu 4%. *Acta Met.,* 1975 ;**23:**1325-1336.
[41] Wei R. P. Some aspects of environment-enhanced fatigue crack growth. *Engineering Fracture Mechanics,* 1968;**1**:633-651.
[42] Bignonet A, Loison D, Namdar-Irani R, Bouchet B, Kwon J.H and Petit J. Environmental and frequency Effects on Near-Threshold Fatigue Crack Propagation in Structural Steels. *Fatigue Crack growth Thresholds Concepts,* Davidson D. and Suresh S. Eds., TMS AIME pub., Philadelphia, PA, USA. 1983:99-114.
[43] Pelloux R. M. N. Crack Extension by Alternate Shear, *Engng. Fract. Mech.,*1970;**1**:697-704.
[44] Petit J, Sarrazin-Baudoux C. Some critical aspects of low rate fatigue crack propagation in metallic materials. Int. Jal of Fat. 2010;**32**:962.
[45] Richard S, Sarrazin-Baudoux C, Petit J and Gasquères C. Coupled influence of microstructure and atmosphere environment on Fatigue Crack Path in new generation Al alloys. To be published in Engineering Fracture Mechanics; 2010.